JOURNAL OF SYNCHROTRON RADIATION

ISSN 1600-5775

Development of variable-magnification X-ray Bragg optics

Keiichi Hirano,* Yoshiki Yamashita, Yumiko Takahashi and Hiroshi Sugiyama

Institute of Materials Structure Science, High Energy Accelerator Research Organization, Tsukuba, Ibaraki 305-0801, Japan. *Correspondence e-mail: keiichi.hirano@kek.jp

Received 23 February 2015
Accepted 6 May 2015

Edited by A. Momose, Tohoku University, Japan

Keywords: X-ray magnifier; variable-magnification; dynamical diffraction; imaging; image processing.

A novel X-ray Bragg optics is proposed for variable-magnification of an X-ray beam. This X-ray Bragg optics is composed of two magnifiers in a crossed arrangement, and the magnification factor, M, is controlled through the azimuth angle of each magnifier. The basic properties of the X-ray optics such as the magnification factor, image transformation matrix and intrinsic acceptance angle are described based on the dynamical theory of X-ray diffraction. The feasibility of the variable-magnification X-ray Bragg optics was verified at the vertical-wiggler beamline BL-14B of the Photon Factory. For X-ray Bragg magnifiers, Si(220) crystals with an asymmetric angle of 14° were used. The magnification factor was calculated to be tunable between 0.1 and 10.0 at a wavelength of 0.112 nm. At various magnification factors ($M \geq 1.0$), X-ray images of a nylon mesh were observed with an air-cooled X-ray CCD camera. Image deformation caused by the optics could be corrected by using a 2×2 transformation matrix and bilinear interpolation method. Not only absorption-contrast but also edge-contrast due to Fresnel diffraction was observed in the magnified images.

1. Introduction

The X-ray Bragg magnifier based on asymmetric diffraction at a nearly perfect crystal (Kohra, 1972) is a useful optical element for X-ray radiology and microscopy, and has been used at synchrotron facilities, for example, for X-ray micro-tomography (μ-CT) (Stampanoni *et al.*, 2002, 2003), analyzer-based phase-contrast imaging (Modregger *et al.*, 2006; Hönnicke & Cusatis, 2007; Hirano, 2011) and inline holography (Vagovič *et al.*, 2013, 2014). One of the most striking features of the X-ray Bragg magnifier is that it can cover a wide range of resolution from submicrometer (Kobayashi *et al.*, 2001; Schäfer & Köhler, 2003) up to submillimeter, thus filling the gap between X-ray microscopy and radiology. Another attractive feature is that it can be combined with X-ray single-photon-counting detectors such as PILATUS (Stampanoni *et al.*, 2005) and Medipix (Vagovič *et al.*, 2013), opening up a new possibility for high-resolution, wide-dynamic-range, high-sensitivity and fast X-ray imaging.

In the conventional X-ray Bragg magnifier, the magnification factor is given by $M = \sin(\theta_B + \alpha)/\sin(\theta_B - \alpha)$, where θ_B is the Bragg angle and α is the angle between the diffracting lattice planes and the crystal surface. From this equation, it can be seen that the only ways to change the magnification factor are either to change the asymmetric angle, α, by replacing the magnifier crystal, or to change the Bragg angle, θ_B, by changing the X-ray wavelength. In either case, tedious procedures of rearranging the optics are required. Due to this lack of flexibility in tuning the magnification factor, use of the X-ray Bragg magnifier has long been hampered. In order to solve

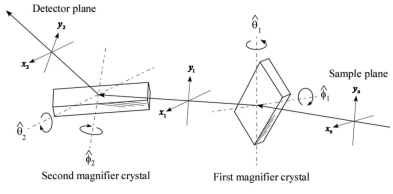

this problem, we developed a variable-magnification X-ray Bragg magnifier by introducing a new rotation axis (the $\hat{\varphi}$-axis) to the conventional Bragg magnifier (Hirano *et al.*, 2014*a*,*b*). Thus it became feasible to locate a region-of-interest (ROI) in a sample under low magnification, and then to observe the details of the ROI under an optimized magnification. Further, our variable-magnification X-ray Bragg magnifier was successfully applied to X-ray computed tomography (CT) (Hirano *et al.*, 2014*a*) and analyzer-based phase-contrast imaging (Hirano *et al.*, 2014*b*). However, our previous studies considered only one-dimensional magnification and demagnification. In this paper, we propose a new variable-magnification X-ray Bragg optics for two-dimensional magnification.

2. Variable-magnification X-ray Bragg optics

Our variable-magnification X-ray Bragg optics consists of two magnifier crystals in a crossed arrangement as schematically shown in Fig. 1. The first crystal magnifies the incident beam in the x_0 direction while the second crystal does so in the y_0 direction. The glancing angle of each crystal, θ_j, is set at the Bragg condition. Here, the subscript j is 1 for the first magnifier and 2 for the second magnifier. The $\hat{\varphi}_j$ axis is perpendicular to the diffracting lattice planes of the jth crystal, and we can scan the azimuth angle, φ_j, keeping the Bragg condition. This kind of diffraction geometry is known as the rotated-inclined geometry (Smither & Fernandez, 1994) and is used for high-heat-load monochromators at SPring-8 (Uruga *et al.*, 1995; Yabashi *et al.*, 1999). The special case of this geometry ($\varphi = 0°$) is known as the inclined geometry (Hrdý, 1992; Khounsary, 1992; Macrander *et al.*, 1992; Lee *et al.*, 1992; Hrdý & Pacherová, 1993), where the magnification factor is fixed at unity. For $\varphi = +90°$ ($\varphi = -90°$), we have the conventional asymmetric situation at low (high) incident angle.

The basic properties of our optics are described by the dynamical theory of X-ray diffraction (Zachariasen, 1945; Batterman & Cole, 1964; Ishikawa & Kohra, 1991; Authier, 2001). In the rotated-inclined diffraction geometry, it is well known that the exit beam has an off-scattering-plane component (Blasdell & Macrander, 1994; Blasdell *et al.*, 1994). However, since this effect is usually smaller than 0.01° in the case of an X-ray Bragg magnifier, here we ignore it for the

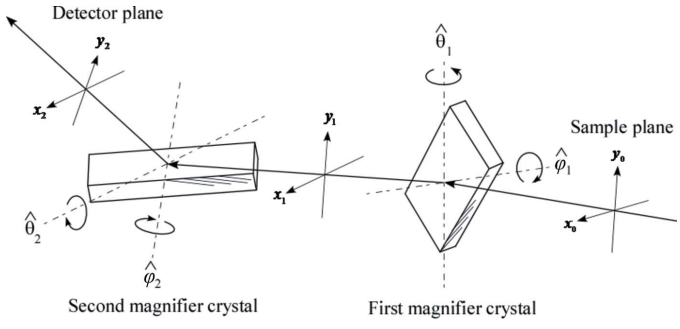

Figure 1
Variable-magnification X-ray Bragg optics.

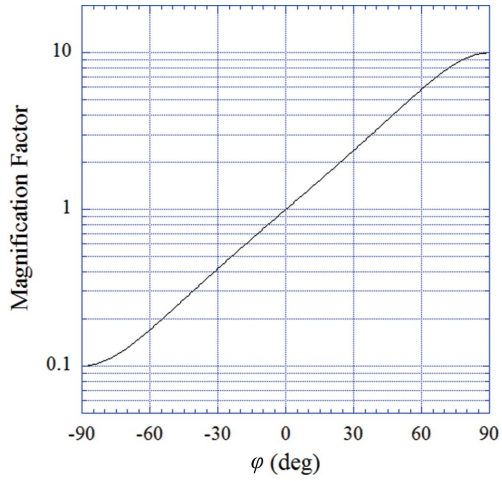

Figure 2
Calculated magnification factor under the following conditions: $\theta_{B1} = \theta_{B2} = 16.96°$, $\alpha_1 = \alpha_2 = 14°$ and $\varphi_1 = \varphi_2 = \varphi$.

sake of simplicity. The effective asymmetric angle, α_j', is given by $\tan\alpha_j' = \tan\alpha_j \sin\varphi_j$; therefore, the magnification factor is given by

$$M_j(\varphi_j) = \frac{\sin(\theta_{Bj} + \alpha_j')}{\sin(\theta_{Bj} - \alpha_j')} = \frac{\cos\alpha_j \sin\theta_{Bj} + \sin\alpha_j \cos\theta_{Bj} \sin\varphi_j}{\cos\alpha_j \sin\theta_{Bj} - \sin\alpha_j \cos\theta_{Bj} \sin\varphi_j}. \quad (1)$$

This equation clearly shows that the magnification factor is tunable through the azimuth angle, φ_j. For example, Fig. 2 shows the calculated magnification factor. Here we set the parameters as follows: $\theta_{B1} = \theta_{B2} = 16.96°$, $\alpha_1 = \alpha_2 = 14°$ and $\varphi_1 = \varphi_2 = \varphi$. In this case the magnification factor varies between 0.1 and 10.

From the viewpoint of the geometrical optics, a point (x_0, y_0) on the sample plane is projected by the first magnifier to a point (x_1, y_1), and then by the second magnifier to a point (x_2, y_2) on the detector plane according to the following equations:

$$\begin{pmatrix} x_1 \\ y_1 \end{pmatrix} = \begin{pmatrix} -M_1 & L_1 \\ 0 & 1 \end{pmatrix} \begin{pmatrix} x_0 \\ y_0 \end{pmatrix}, \quad (2)$$

$$\begin{pmatrix} x_2 \\ y_2 \end{pmatrix} = \begin{pmatrix} 1 & 0 \\ -L_2 & -M_2 \end{pmatrix} \begin{pmatrix} x_1 \\ y_1 \end{pmatrix}, \quad (3)$$

where

$$L_j(\varphi_j) = \tan\alpha_j \cos\alpha_j' \frac{\sin(2\theta_{Bj})}{\sin(\theta_{Bj} - \alpha_j')} \cos\varphi_j. \quad (4)$$

Combining equations (2) and (3) we obtain

$$\begin{pmatrix} x_2 \\ y_2 \end{pmatrix} = \begin{pmatrix} -M_1 & L_1 \\ L_2 M_1 & -L_1 L_2 - M_2 \end{pmatrix} \begin{pmatrix} x_0 \\ y_0 \end{pmatrix}. \quad (5)$$

For example, let us assume that the shape of the incident beam on the sample plane is square as shown in Fig. 3(*a*). Fig. 3(*b*) shows calculated beam shapes on the detector plane for

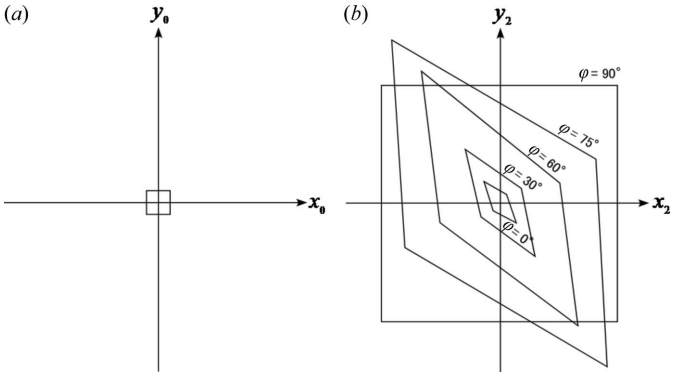

Figure 3
Shape of the beam (*a*) on the sample plane and (*b*) on the detector plane. The calculation conditions were the same as for Fig. 2.

various azimuth angles under the same conditions as Fig. 2. It is clearly seen that, due to the non-diagonal components of the transformation matrix in equation (5), the square beam is deformed by the optics to the parallelogram beam except at $\varphi_j = \pm 90°$. However, in modern X-ray imaging with the widespread use of X-ray digital area sensors such as X-ray CCD cameras and flat panel sensors, we can easily correct this image deformation using equation (5). Note that the above discussion is based on the geometrical optics; therefore, equation (5) is not valid in the wave optical region.

The throughput of the optics depends on the intrinsic acceptance angle of each magnifier which is given by

$$\omega_{0j} = \sqrt{M_j}\,\omega_j, \tag{6}$$

where ω_j is the full width at half-maximum (FWHM) of the rocking curve of the jth magnifier for the symmetric diffraction and is given by

$$\omega_j \approx \frac{2}{\sin(2\theta_{Bj})}\frac{r_e\lambda^2}{\pi V_j}|C_j||F_{hj}|, \tag{7}$$

where r_e is the classical electron radius, λ is the wavelength, V_j is the volume of the unit cell, C_j is the polarization factor and F_{hj} is the crystal structure factor. The polarization factor, C_j, is 1 for the σ-polarization and $\cos(2\theta_{Bj})$ for the π-polarization.

The intrinsic angular divergence of the outgoing beam is given by

$$\omega_{Hj} = \omega_j/\sqrt{M_j}. \tag{8}$$

Note that the intrinsic angular divergence, ω_{Hj}, is not equivalent to the actual angular divergence, $\Delta\theta_{Hj}$, for a polychromatic source (Brauer *et al.*, 1995*a*,*b*). Due to the polychromatic nature of the synchrotron radiation, the beam properties such as coherence depend on $\Delta\theta_{Hj}$. The actual angular divergence, $\Delta\theta_{Hj}$, can be estimated based on the DuMond diagram (DuMond, 1937).

Because each magnifier functions independently, we can assume that the spatial resolution in the x_2 direction depends on the first magnifier, while that in the y_2 direction on the second one. The image blurring in each direction originates from several factors such as the so-called penumbral blurring, the diffractive blurring caused by the X-ray penetration into the magnifier, the blurring due to the detector and so on (Hirano *et al.*, 2014*a*).

3. Experiments and results

In order to verify the feasibility of our variable-magnification X-ray Bragg optics, we performed experiments at the vertical-wiggler beamline BL-14B of the Photon Factory. The experiments were carried out only for the magnification-case ($M \geq 1.0$). At first, the white beam from the light source was monochromated at 0.112 nm by a Si(111) double-crystal monochromator. Then the monochromatic beam linearly polarized in the vertical direction was incident to the variable-magnification X-ray Bragg optics. The polarization of the incident beam corresponded to σ-polarization for the first magnifier and π-polarization for the second magnifier. For magnifiers, we used asymmetric Si(220) crystals ($\theta_{B1} = \theta_{B2} = 16.96°$, $\alpha_1 = \alpha_2 = 14°$) made of non-doped float-zone silicon crystal ($\rho \geq 2000\ \Omega$ cm). The surface of the magnifier crystals was mechanochemically polished in order to remove defects and strain fields. The intrinsic acceptance angle was calculated to be $3.6''\sqrt{M_1}$ for the first magnifier and $3.0''\sqrt{M_2}$ for the second magnifier. Fig. 4 shows a photograph of the first magnifier crystal at $\varphi_1 = 0°$. The $\hat{\theta}_1$ axis was in the vertical direction. The φ_1 stage was mounted on the θ_1-stage so that the $\hat{\varphi}_1$ axis would always become perpendicular to the $\hat{\theta}_1$ axis, and perpendicular to the incident beam at $\theta_1 = 0°$. A two-axis tilt stage was mounted on the φ_1 stage, with which we carefully aligned the orientation of the magnifier so that the diffracting lattice planes would become perpendicular to the $\hat{\varphi}_1$ axis with an accuracy of a few arcseconds. Thus we could scan the azimuth angle, φ_1, without losing the Bragg diffraction. A

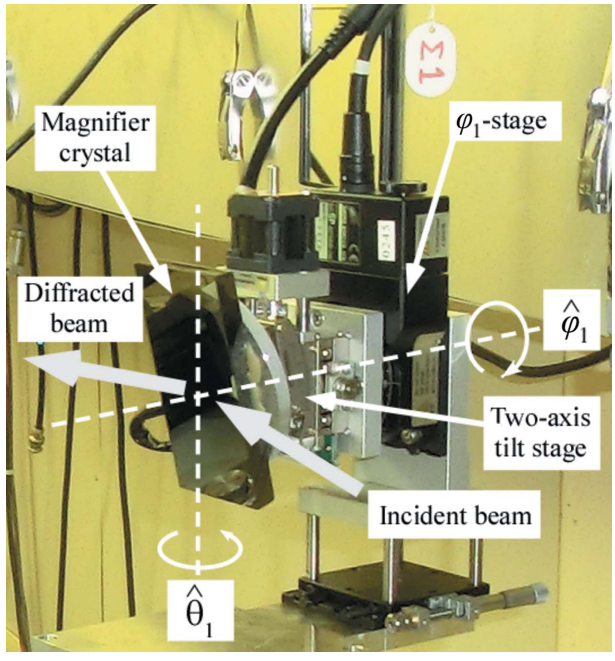

Figure 4
Photograph of the first magnifier crystal at $\varphi_1 = 0°$.

similar instrument was also used for the second magnifier crystal. Magnified X-ray images were observed by a fiber-coupled X-ray CCD camera (Photonic Science Ltd, X-ray Coolview FDI 40mm) consisting of a GdO_2S:Tb scintillator, a 3.43:1.00 glass fiber plate and a CCD. At the scintillator, X-rays were converted to visible light, which was transmitted through the glass fiber plate and detected by the CCD. The effective pixel size was 23 µm (H) × 23 µm (V) and the number of pixels was 1384 (H) × 1032 (V).

At first we estimated the spatial resolution of the optics at several magnification factors using MTF charts. The results were almost the same as the previous results obtained for the one-dimensional magnification optics (Hirano *et al.*, 2014*a*). The main determining factors of the spatial resolution were the effective pixel size of the X-ray CCD camera and the penumbral blurring. The penumbral blurring is given by $\Delta x_p \approx sD_{ss}/D_{sd}$, where s is the source size, D_{ss} is the distance between the light source and the sample and D_{sd} is that between the sample and the detector. In our experiments, D_{ss} was about 20 m and D_{sd} was about 1.2 m. The spatial resolution in the vertical direction was slightly better than that in the horizontal direction because of the flat shape of the electron beam. For example, the spatial resolution was estimated to be about 15 µm in the vertical direction and 20 µm in the horizontal direction at $M_1 = M_2 = 5.9$ ($\varphi_1 = \varphi_2 = 60^\circ$).

As a sample we observed a nylon mesh, the period of which was about 1.1 mm in both the horizontal and vertical directions. Fig. 5(*a*) shows a raw image of the sample observed by the X-ray CCD camera at $\varphi_1 = \varphi_2 = 60^\circ$ ($M_1 = M_2 = 5.9$) with an exposure time of 4 s. The raw image is deformed by the optics. Fig. 5(*b*) shows an image corrected by equation (5) and the bilinear interpolation method. For comparison, Fig. 5(*c*) shows a non-deformed magnified image observed at $\varphi_1 = \varphi_2 = 90^\circ$ ($M_1 = M_2 = 10.0$) with an exposure time of 8 s. The shape of the corrected image in Fig. 5(*b*) is almost the same as that of the non-deformed magnified image in Fig. 5(*c*). This shows that the image correction by equation (5) and the bilinear interpolation method was successful. It is worth noting that not only absorption-contrast but also edge-contrast due to Fresnel diffraction is observed in both Figs. 5(*b*) and 5(*c*). The number of observed Fresnel fringe was one in both the horizontal and vertical directions, and finer fringes were not observed. This is due to the moderate spatial resolution described above.

During the course of the azimuth scan, we observed multiple Bragg diffractions at several points where the crystal did not work as a magnifier. We need to keep the azimuth angle away from these angles in order to obtain a normal magnified image. For this purpose, a so-called 'glitch map' (Cole *et al.*, 1962) is helpful. This glitch map is also useful in determining the origin of the azimuth angle for precise image correction.

The throughput of the optics can be improved by replacing the asymmetric silicon crystals with asymmetric germanium crystals. For example, let us assume that the asymmetric Si(220) crystals ($\alpha_1 = \alpha_2 = 14^\circ$, $\theta_{B1} = \theta_{B2} = 16.96^\circ$) are replaced by asymmetric Ge(220) crystals ($\theta_{B1} = \theta_{B2} = 16.26^\circ$). In order to secure the same range of magnification factor ($0.1 \leq M_j \leq 10.0$), the asymmetric angle of the Ge(220) crystals must be set at $\alpha_1 = \alpha_2 = 13.42^\circ$. The intrinsic acceptance angle is calculated to be $6.8''\sqrt{M_1}$ for the first magnifier and $5.8''\sqrt{M_2}$ for the second magnifier. This means that the total throughput of the germanium magnifiers is increased by 265% compared with that of the silicon magnifiers.

In the experiment we could control the magnification factor from 1.0 up to 10 with reasonable throughput even at a second-generation synchrotron radiation facility such as the Photon Factory. In fact, the exposure time was as short as 10 s at the maximum magnification factor ($M_1 = M_2 = 10$). A much wider range of magnification factor will be realised at third-generation synchrotron radiation facilities where submicrometer resolutions have already been achieved with the conventional fixed-magnification X-ray Bragg optics (Kobayashi *et al.*, 2001; Schäfer & Köhler, 2003). We expect that the performance of our variable-magnification X-ray Bragg optics will be maximized at linac-based X-ray sources such as X-ray free-electron lasers (McNeil & Thompson, 2010) and energy-recovery linacs (Levi, 2002), which can produce diffraction-limited X-rays in both the horizontal and vertical directions.

In this paper we demonstrated the X-ray beam magnification in view of controlling the spatial resolution and field of

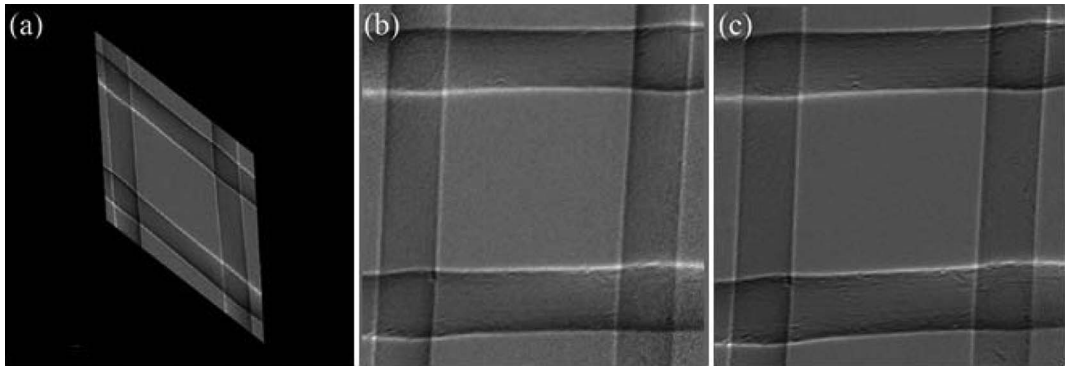

Figure 5
(*a*) Deformed magnified image and (*b*) corrected magnified image of the nylon mesh obtained at $\varphi_1 = \varphi_2 = 60^\circ$ ($M_1 = M_2 = 5.9$). (*c*) Non-deformed magnified image of the sample obtained at $\varphi_1 = \varphi_2 = 90^\circ$ ($M_1 = M_2 = 10.0$). The period of the nylon mesh was about 1.1 mm in both the horizontal and vertical directions.

view of the optical system. Another important usage of the X-ray Bragg magnifier is beam demagnification (condensation) for micro-beam production (Tsusaka *et al.*, 2000). Our X-ray Bragg optics opens up a new possibility for producing a variable-size micro-beam. Unlike other focusing elements such as Fresnel zone plates (Baez, 1960), compound refractive lenses (Schroer *et al.*, 2005), Kirkpatrick–Baez mirrors (Kirkpatrick & Baez, 1948) and capillaries (Nakazawa, 1983), our variable-magnification X-ray Bragg optics does not cause serious deterioration in beam parallelity. Thanks to this advantage, our X-ray optics will be useful for investigating the defects and strain fields in electric devices by micro-beam diffraction experiments.

4. Conclusion

We have developed a novel variable-magnification X-ray Bragg optics composed of two magnifiers in a crossed arrangement. Based on the dynamical theory of X-ray diffraction, we described the basic properties of the optics such as the magnification factor, image transformation matrix and intrinsic acceptance angle. In the feasibility test performed at the vertical-wiggler beamline BL-14B of the Photon Factory, we could control the magnification factor between 1.0 and 10 with reasonable throughput at the wavelength of 0.112 nm. Furthermore, we could successfully correct the image deformation caused by the optics using the image transformation matrix and bilinear interpolation method.

Acknowledgements

This work was performed with the approval of the Program Advisory Committee of the Photon Factory (2013G054 and 2014G021).

References

Authier, A. (2001). *Dynamical Theory of X-ray Diffraction*. Oxford University Press.
Baez, A. V. (1960). *Nature (London)*, **186**, 958.
Batterman, B. W. & Cole, H. (1964). *Rev. Mod. Phys.* **36**, 681–717.
Blasdell, R. C. & Macrander, A. T. (1994*a*). *Nucl. Instrum. Methods Phys. Res. A*, **347**, 320–323.
Blasdell, R. C., Macrander, A. T. & Lee, W. K. (1994*b*). *Nucl. Instrum. Methods Phys. Res. A*, **347**, 327–330.
Brauer, S., Stephenson, G. B., Mochrie, S. G. J., Dierker, S. B., Fleming, R. M., Pindak, R., Robinson, I. K., Grubel, G., Als-Nielsen, J. & Abernathy, D. L. (1995*a*). *Rev. Sci. Instrum.* **66**, 1506–1509.
Brauer, S., Stephenson, G. B. & Sutton, M. (1995*b*). *J. Synchrotron Rad.* **2**, 163–173.
Cole, H., Chambers, F. H. & Dunn, H. M. (1962). *Acta Cryst.* **15**, 138–144.
DuMond, J. W. M. (1937). *Phys. Rev.* **52**, 872–883.
Hirano, K. (2011). *Jpn. J. Appl. Phys.* **50**, 026402.
Hirano, K., Takahashi, Y. & Sugiyama, H. (2014*a*). *Nucl. Instrum. Methods Phys. Res. A*, **741**, 78–83.
Hirano, K., Takahashi, Y. & Sugiyama, H. (2014*b*). *Jpn. J. Appl. Phys.* **53**, 040302.
Hönnicke, M. G. & Cusatis, C. (2007). *Rev. Sci. Instrum.* **78**, 113708.
Hrdý, J. (1992). *Rev. Sci. Instrum.* **63**, 459–460.
Hrdý, J. & Pacherová, O. (1993). *Nucl. Instrum. Methods Phys. Res. A*, **327**, 605–611.
Ishikawa, T. & Kohra, K. (1991). *Handbook on Synchrotron Radiation*, Vol. 3, edited by G. S. Brown and D. E. Moncton, pp. 63–104. Amsterdam: North-Holland.
Khounsary, A. M. (1992). *Rev. Sci. Instrum.* **63**, 461–464.
Kirkpatrick, P. & Baez, A. V. (1948). *J. Opt. Soc. Am.* **38**, 766–773.
Kobayashi, K., Izumi, K., Kimura, H., Kimura, S., Ibuki, T., Yokoyama, Y., Tsusaka, Y., Kagoshima, Y. & Matsui, J. (2001). *Appl. Phys. Lett.* **78**, 132–134.
Kohra, K. (1972). *Proceedings of the Sixth International Conference on X-ray Optics and Microscopy*, edited by G. Shinoda, K. Kohra and T. Ichinokawa, pp. 35–45. University of Tokyo Press.
Lee, W. K., Macrander, A. T., Mills, D. M., Rogers, C. S., Smither, R. K. & Berman, L. E. (1992). *Nucl. Instrum. Methods Phys. Res. A*, **320**, 381–387.
Levi, B. G. (2002). *Phys. Today*, **55**, 23–25.
McNeil, B. W. J. & Thompson, N. R. (2010). *Nat. Photon.* **4**, 814–821.
Macrander, A. T., Lee, W. K., Smither, R. K., Mills, D. M., Rogers, C. S. & Khounsary, A. M. (1992). *Nucl. Instrum. Methods Phys. Res. A*, **319**, 188–196.
Modregger, P., Lübbert, D., Schäfer, P. & Köhler, R. (2006). *Phys. Rev. B*, **74**, 054107.
Nakazawa, H. (1983). *J. Appl. Cryst.* **16**, 239–241.
Schäfer, P. & Köhler, R. (2003). *J. Phys. D*, **36**, A113–A117.
Schroer, C. G., Kupanov, O., Patommel, J., Boye, P., Feldkamp, J., Lengeler, B., Burghammer, M., Riekel, C., Vincze, L., Hart, A. & Küchler, M. (2005). *Appl. Phys. Lett.* **87**, 124103.
Smither, R. K. & Fernandez, P. B. (1994). *Nucl. Instrum. Methods Phys. Res. A*, **347**, 313–319.
Stampanoni, M., Borchert, G. & Abela, R. (2005). *Nucl. Instrum. Methods Phys. Res. A*, **551**, 119–124.
Stampanoni, M., Borchert, G., Abela, R. & Rüegsegger, P. (2002). *J. Appl. Phys.* **92**, 7630–7635.
Stampanoni, M., Borchert, G., Abela, R. & Rüegsegger, P. (2003). *Appl. Phys. Lett.* **82**, 2922–2924.
Tsusaka, Y., Yokoyama, K., Takeda, S., Urakawa, M., Kagoshima, Y., Matsui, J., Kimura, S., Kimura, H., Kobayashi, K. & Izumi, K. (2000). *Jpn. J. Appl. Phys.* **39**, L635–L637.
Uruga, T., Kimura, H., Kohmura, Y., Kuroda, M., Nagasawa, H., Ohtomo, K., Yamaoka, H., Ishikawa, T., Ueki, T., Iwasaki, H., Hashimoto, S., Kashihara, Y. & Okui, K. (1995). *Rev. Sci. Instrum.* **66**, 2254–2256.
Vagovič, P., Korytár, D., Cecilia, A., Hamann, E., Švéda, L., Pelliccia, D., Härtwig, J., Zápražný, Z., Oberta, P., Dolbnya, I., Shawney, K., Fleschig, U., Fiederle, M. & Baumbach, T. (2013). *J. Synchrotron Rad.* **20**, 153–159.
Vagovič, P., Švéda, L., Cecilia, A., Hamann, E., Pelliccia, D., Gimenez, E. N., Korytár, D., Pavlov, K. M., Zápražný, Z., Zuber, M., Koenig, T., Olbinado, M., Yashiro, W., Momose, A., Fiederle, M. & Baumbach, T. (2014). *Opt. Express*, **22**, 21508–21520.
Yabashi, M., Yamazaki, H., Tamasaku, K., Goto, S., Takeshita, K., Mochizuki, T., Yoneda, Y., Furukawa, Y. & Ishikawa, T. (1999). *Proc. SPIE*, **3773**, 2–13.
Zachariasen, W. H. (1945). *Theory of X-ray Diffraction in Crystals*. New York: Wiley.